Energy Materials and Devices

Research Article

Effects of interface parameters on the transport properties of nanocomposites

Tinggang Zhang ✉

Graphical Abstract

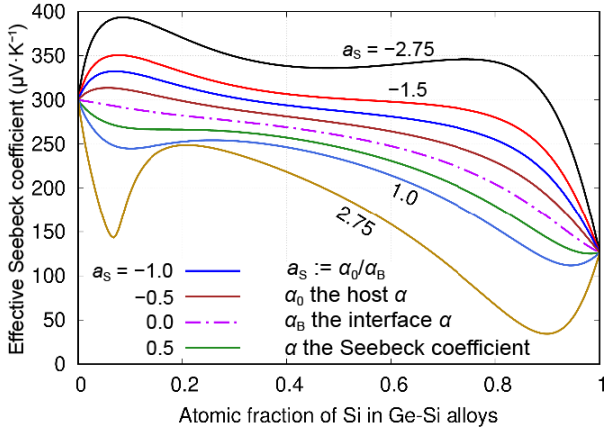

The effects of interface parameters, such as thermal and electrical barrier resistance and interface Seebeck coefficient, on the transport properties of nanocomposites, including the thermal and the electrical conductivity, the Seebeck coefficient, and the Hall mobility, were investigated using the effective medium approximations. The results showed that these transport properties could be further improved through optimizing the interface parameters of nanocomposites.

✉Address correspondence to Tinggang Zhang, zhangtinggang84@gmail.com

Received: January 28, 2024
Revised: February 22, 2024
Accepted: February 26, 2024

Citation: Zhang T. Effects of interface parameters on the transport properties of nanocomposites. *Energy Mater. Devices*, 2024, 2(2), 9370028. https://doi.org/10.26599/EMD.2024.9370028

Energy Materials and Devices

Open Access

Research Article

https://doi.org/10.26599/EMD.2024.9370028

Effects of interface parameters on the transport properties of nanocomposites

Tinggang Zhang[1,2] ✉

[1] *Formerly at University of Alaska Fairbanks, Fairbanks, Alaska 99775, USA*
[2] *211 Clarkson Drive Apt 7, Fairbanks, Alaska 99709, USA*

Received: January 28, 2024 / **Revised:** February 22, 2024 / **Accepted:** February 26, 2024

ABSTRACT

This study introduces a continuum medium approximation (CMA) and an empirical effective medium approximation (EMA)-type formulation to estimate the transport properties, including electrical conductivity, thermal conductivity, Seebeck coefficient, and Hall mobility, of nanostructured composites. The CMA incorporates the interface parameters mediated by newly introduced distribution functions to resolve predictions that deviate from the inclusion properties at its volume fraction of 1 in current EMAs and yields predictions agreed well with both the empirical EMA and experimental data. The empirical EMA-type formulation resolves the differences in CMA predictions for the media $A_{1-x}B_x$ and $B_{1-x}A_x$ and provides a unique prediction that agrees very well with experimental data at a given volume fraction ranging from 0 to 1. The effects of the interface parameters on the transport properties were investigated. The results indicated that the efficiency of nanostructured composites could be further improved by optimizing the interface parameters.

KEYWORDS

continuum medium approximation, thermal barrier resistance, electrical barrier resistance, host–particle interface density, distribution function of interface parameter

1 Introduction

Effective medium approximation (EMA) has been used to predict the transport properties of nanostructured thermoelectric composites and to investigate the roles played by different phases of a composite and the mechanisms introduced by nanostructures to improve properties for enhanced energy conversion efficiency. Based on EMA and Kapitza thermal contact resistance[1], Nan et al. developed a comprehensive EMA-based formulation that contains the interfacial thermal resistance to determine the effective thermal conductivity of arbitrary particulate composites[2]. The formulation ignored the interparticle phonon scattering, thus can be applicable to composites with a small volume fraction of inclusion. Nanocomposites can often contain much higher volume fractions of nanograins, and their particle size can decrease to the order of phonon wavelength and mean free path (MFP). Therefore, both the interfacial scattering of phonons and the interparticle phonon scatterings need to be accounted for in an EMA. The modified EMAs by Minnich and Chen[3] and Poon and Limtragool[4] accounted for both the interfacial and the interparticle phonon scatterings. Nan's EMA and a classical EMA formulation were used by Hao et al. along with their atomistic simulations to investigate the thermal conductivity of aligned Ge nanowires embedded in a crystalline Si matrix[5]. The classical EMA formulation was applied to three phases, namely Ge, Si, and the thermal boundary phase which contains both germanium and silicon elements. The thermal conductivity of the thermal boundary phase originated from the mismatch of group velocities of phonons on different sides of the interface, leading to strong phonon scattering and changes in the effective thermal conductivity. Based on Bruggeman formulation and Boltzmann transport equation, Sonntag developed the EMA formulations for both the thermal conduc-

✉ Address correspondence to Tinggang Zhang, zhangtinggang84@gmail.com

tivity and the Seebeck coefficient of thermoelectric composites[6]. The formulation was late modified by Kyratsi et al. to study the amorphous or crystalline β-$K_2Bi_8Se_{13}$ nanocomposites[7]. They used four phases, that is, nanocrystallites, microcrystallites, amorphous phase, and pores in the prediction and the results agreed well with the experimental data. A general EMA combined with percolation theory[8] alongside with the EMA developed by Bergman and Levy[9] were used by Sharma et al. to investigate the composite of $AgSbTe_2$ embedded with Sb_2Te_3 nanoinclusions[10]. The results showed that morphology of the inclusions significantly influenced the effective transport properties. To investigate the experimental findings that showed pores entrapped in a thermoelectric material could lower thermal conductivity considerably and improve figure of merit (zT)[11, 12], Lee et al. used EMAs and quantum mechanics to calculate the transport properties of porous Si-Ge[13]. The result showed that the charge carriers were scattered more severely in nanograined materials compared with macroscale porous materials due to a larger number density of scattering sites. Porous nanograined materials can enhance the Seebeck coefficient due to the energy filtering effect and lower the thermal conductivity, however, these materials can also lower the electrical conductivity. Porous materials have wide applications in batteries and energy conversion devices. Ion transport in porous electrodes was studied by Tao et al. using molecular dynamics simulations combined with EMA[14].

Thermal barrier resistance, particle size and shape, and host–particle interface density are recognized as the key parameters in determining the thermal conductivity of a nanocomposite. Standard EMAs do not include these interface parameters in the formulations. Consequently, their predictions can only vary between the properties of the single-phased materials and could differ considerably from experimental data, as illustrated by the blue line in Fig. 1. EMAs incorporated with the interface parameters and using constant properties for the host and the particle improved the predictions such that they may exceed the properties of both the host and the particle, as shown by the red line in Fig. 1. EMAs that include the interface parameters and use the properties dependent on the host–particle interface density and particle size for both the host and the particle made considerable improvement on the predictions that closely align with experimental data as illustrated by the black line in Fig. 1.

However, the presence of these interface parameters in EMAs results in that the predictions deviate from the particle properties at its volume fraction of 1 and that the differences between the approximations for $A_{1-x}B_x$ and $B_{1-x}A_x$ increase. In this work, a continuum medium approximation (CMA) for the

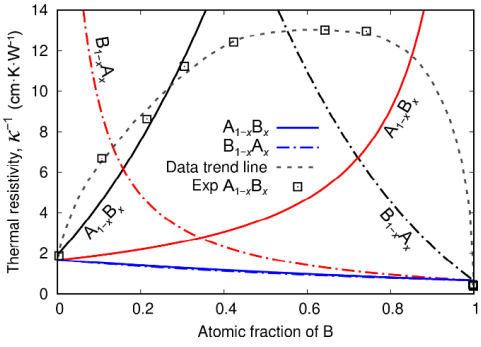

Figure 1 Diagram shows advances of EMAs. The lower bottom curves represent the results from standard EMAs that do not include the interface parameters, i.e., thermal barrier resistance, particle size, and host–particle interface density, while the EMAs of the curves above them do include those parameters.

transport properties (electrical conductivity, thermal conductivity, Seebeck coefficient, and Hall coefficient) is developed using the continuum equation along with smeared property approximation and perturbation theory. This CMA is incorporated with the interface parameters that are mediated by the newly proposed distribution functions to resolve the predictions that deviate at the volume fraction of 1. An empirical EMA-type formulation is then introduced to unify the CMA predictions for $A_{1-x}B_x$ and $B_{1-x}A_x$ to give a unique prediction within the volume fraction ranging from 0 to 1. Numerical calculations carried out for both undoped and doped Ge–Si alloys are compared with experimental data. The effects of the interface parameters on the transport properties of the alloys are illustrated.

2 Formulation outline

The presence of the Kapitza thermal boundary resistance and the electrical boundary impedance at the interface between the continuous phase (host) and the inclusions (particles) embedded in the continuous phase of a composite leads to the discontinuities of temperature, electrical potential, and their respective currents. These interface effects were not accounted for in existing formulations[15] for the transport properties of inhomogeneous materials using the continuum medium theory. As the volume fraction of the particle increases and its size decreases to an order of magnitude comparable to the wavelength, the interface effects are likely to become highly significant for transport in nanostructured composites. To maintain the continuum medium theory valid for approximating the transport properties of nanostructured composites, a smeared property approximation is used to ensure the continuity of temperature, electrical potential, and their respective currents across the interface. The method is based on the concept that the reduction in the particle size and the increase in the host–particle interface

density alter the transport trajectory of energy carriers in both the host medium and the particle, leading to changes in their bulk properties. Let's start with the thermal conductivity. The increase in the interface density induces a small change, denoted as $\Delta\kappa_0$, in the thermal conductivity of the host medium. The resulting thermal conductivity is $\kappa_0' = \kappa_0 + \Delta\kappa_0$. Since the interface phase contains both the host medium and the inclusion, a smeared property is used to simply approximate the $\Delta\kappa_0$, i.e., $\Delta\kappa_0 = \frac{\kappa_i \kappa_0 R_{\text{th}}}{a} = \alpha_{\text{th}}\kappa_i$, where κ_{i} is the thermal conductivity of the inclusion, R_{th} is the thermal barrier resistance, and a is a radius. The resulting thermal conductivity becomes $\kappa_0' = \kappa_0 + \alpha_{\text{th}}\kappa_i$. The CMA of the effective thermal conductivity is then given by:

$$\kappa_{\text{p}} = \kappa_0 \left\{1 + 2\phi_i \left[\frac{\kappa_i'(1-\alpha_{\text{th}}) - \kappa_0}{\kappa_i'(1+2\alpha_{\text{th}}) + 2\kappa_0}\right]\right\}\left\{1 - \phi_i \left[\frac{\kappa_i'(1-\alpha_{\text{th}}) - \kappa_0}{\kappa_i'(1+2\alpha_{\text{th}}) + 2\kappa_0}\right]\right\}^{-1} - 2\sigma_0 T \left\{\left[1 - \phi_i \left(\frac{\kappa_i'(1-\alpha_{\text{th}}) - \kappa_0}{\kappa_i'(1+2\alpha_{\text{th}}) + 2\kappa_0}\right)\right]^{-1}\right.$$
$$\left.\left[\frac{3\phi_{\text{i}}(\alpha_{\text{i}} - \alpha_0)\sigma_i}{\sigma_i(1+2\alpha_{\text{el}}) + 2\sigma_0}\right]\left[\frac{3\kappa_0(1+\alpha_{\text{th}}\kappa_i/\kappa_0)}{\kappa_i'(1+2\alpha_{\text{th}}) + 2\kappa_0}\right]\right\}^2 \cdot \left\{\left[2 + \phi_i \left(\frac{\sigma_i(1-\alpha_{\text{el}}) - \sigma_0}{\sigma_i(1+2\alpha_{\text{el}}) + 2\sigma_0}\right)\right]\left[1 + 2\phi_{\text{i}} \left(\frac{\sigma_i(1-\alpha_{\text{el}}) - \sigma_0}{\sigma_i(1+2\alpha_{\text{el}}) + 2\sigma_0}\right)\right]\right\}^{-1} \quad (1a)$$

where κ_i' is the change of the thermal conductivity caused by the Peltier effect at the host–particle interface and is given by:

$$\kappa_i' = \kappa_i + \frac{2\sigma_i\sigma_0}{\sigma_i + 2\sigma_0}(\alpha_i - \alpha_0)^2 \quad (1b)$$

where σ_0 and σ_i are the electrical conductivity of the host and the particle, respectively, α_0 and α_i are the Seebeck coefficients of the host and the i_{th} particle, respectively, ϕ_i is the volume fraction of the inclusion, and α_{el} is the coefficient of the electrical barrier resistance to be defined subsequently. The first term on the right side of Eq. (1a) is the same as Nan's formulation for spherical inclusions. Equation (1a) also accounts for the Peltier effect at the host–particle interface by the second term on the right side of the equation.

The kinetic theory-based bulk properties of the host and the particle, and the thermal barrier resistance introduced in Chen and Minnich's work[3], are used in Eq. (1a) to account for the effects of particle size and the host–particle interface density on these bulk properties. These properties are calculated, respectively, by:

$$\kappa_x = \frac{1}{3} C_{\text{p}_x} \nu_x \Lambda_x \quad (1c)$$

$$R_{\text{th}} = \frac{4 f_{\text{Rd}} (C_{\text{p}_1}\nu_1 + C_{\text{p}_2}\nu_2)}{C_{\text{p}_1}\nu_1 C_{\text{p}_2}\nu_2} \quad (1d)$$

where the subscript x is 0 for the host medium and i for the inclusion, C_{p} is the specific heat capacity, ν the phonon group velocity, Λ the phonon mean free path (MFP), and f_{Rd} is a distribution function of the thermal barrier resistance. For the host medium, the effective MFP is given by:

$$\frac{1}{\Lambda_{\text{eff}}} = \frac{1}{\Lambda_0} + \frac{\Phi_{\text{d}}}{4} \quad (1e)$$

where Φ_{d} is a distribution function of the host–particle interface density for spherical inclusions. For nanoparticles, the MFP is given by:

$$\frac{1}{\Lambda_{\text{eff}}} = \frac{1}{\Lambda_i} + \frac{1}{d} \quad (1f)$$

where d is the particle diameter.

The distribution functions, f_{Rd} and Φ_{d}, should meet the conditions that the host–particle interface density or the thermal barrier resistance is 0 when the volume fraction of inclusion is 0 or 1. To meet these requirements, the distribution function for the interface density is introduced in the following form:

$$\phi_1 \frac{X_1^{m_{\text{h}}} - X_{\text{e}}^{m_{\text{h}}}}{X_1^{m_{\text{h}}} - r_{\text{B}} X_{\text{e}}^{m_{\text{h}}}} + \phi_2 \frac{X_2^{m_{\text{h}}} - X_{\text{e}}^{m_{\text{h}}}}{X_2^{m_{\text{h}}} - r_{\text{A}} X_{\text{e}}^{m_{\text{h}}}} = 0 \quad (1g)$$

where ϕ_1 is the volume fraction of inclusion; $\phi_2 = 1 - \phi_1$, $X_1 = \phi_1$, $X_2 = \phi_2$, X_{e} is Φ_{d}, and r_{A}, r_{B}, and m_{h} are the empirical parameters to be determined through correlation with experimental data.

The distribution function for the thermal barrier resistance is defined as:

$$f_{\text{Rd}} = [4\phi_1(1-\phi_1)]^{m_{\text{k}}} \quad (1h)$$

where m_{k} is an empirical parameter. Since the differential equations for the continuum medium are the same for both electrical conduction and heat transport and differ only in their constants and independent variables, following the same treatment for the effective thermal conductivity, the effective electrical conductivity can be obtained:

$$\sigma_{\text{p}} = \sigma_0 \frac{1 + 2\phi_i \frac{\sigma_i(1-\alpha_{\text{el}}) - \sigma_0}{\sigma_i(1+2\alpha_{\text{el}}) + 2\sigma_0}}{1 - \phi_i \frac{\sigma_i(1-\alpha_{\text{el}}) - \sigma_0}{\sigma_i(1+2\alpha_{\text{el}}) + 2\sigma_0}} \quad (2a)$$

in which $\alpha_{\text{el}} = f_{\text{sd}}\alpha_{\text{el}}^0$ and $\alpha_{\text{el}}^0 = \frac{R_{\text{el}}\sigma_0}{a}$ where R_{el} is the electrical barrier resistance, a is the radius and f_{sd} is a distribution function of the electrical barrier resistance given by:

$$\phi_1 \frac{X_1^{m_{\text{s}}} - X_{\text{e}}^{m_{\text{s}}}}{X_1^{m_{\text{s}}} - r_{\text{B}} X_{\text{e}}^{m_{\text{s}}}} + \phi_2 \frac{X_2^{m_{\text{s}}} - X_{\text{e}}^{m_{\text{s}}}}{X_2^{m_{\text{s}}} - r_{\text{A}} X_{\text{e}}^{m_{\text{s}}}} = 0 \quad (2b)$$

in which X_{e} is f_{sd}, s_{A}, s_{B}, and m_{s} are empirical parameters to be determined through correlation with experimental data.

Subsequently, the CMA for the effective Seebeck coefficient can be expressed as:

$$\alpha_p = \alpha_0 + \frac{\left[\frac{3\sigma_i}{\sigma_i(1+2\alpha_{el})+2\sigma_0}\right]\left[\frac{3\kappa_0(1+\alpha_{el}\sigma_i)}{\kappa_i'(1+2\alpha_{th})+2\kappa_0}\right][\alpha_i(1-\alpha_{a_S})-\alpha_0]\phi_i}{\left\{1+2\phi_i\left[\frac{\sigma_i(1-\alpha_{el})-\sigma_0}{\sigma_i(1+2\alpha_{el})+2\sigma_0}\right]\right\}\left\{1-\phi_i\left[\frac{\kappa_i'(1-\alpha_{th})-\kappa_0}{\kappa_i'(1+2\alpha_{th})+2\kappa_0}\right]\right\}} \tag{3a}$$

in which $\alpha_{a_S} = f_{a_Sd}a_S$ where f_{a_Sd} is a distribution function of the interface Seebeck coefficient ratio, and $a_S = \alpha_0/\alpha_B$, α_B is the boundary Seebeck coefficient[16]. f_{a_Sd} is given by:

$$\frac{\phi_1(X_1^{m_{a_S}} - X_e^{m_{a_S}})}{X_1^{m_{a_S}} - a_{SB}X_e^{m_{a_S}}} + \frac{\phi_2(X_2^{m_{a_S}} - X_e^{m_{a_S}})}{X_2^{m_{a_S}} - a_{SA}X_e^{m_{a_S}}} = 0 \tag{3b}$$

$$R_{H_p} = R_{H_0}\left[\frac{1-\phi_i\frac{\sigma_i(1-\alpha_{el})-\sigma_0}{\sigma_i(1+2\alpha_{el})+2\sigma_0}}{1+2\phi_i\frac{\sigma_i(1-\alpha_{el})-\sigma_0}{\sigma_i(1+2\alpha_{el})+2\sigma_0}}\right]^2 + 9\left[1+2\phi_i\frac{\sigma_i(1-\alpha_{el})-\sigma_0}{\sigma_i(1+2\alpha_{el})+2\sigma_0}\right]^{-2}\frac{\sigma_i^2R_{H_i} - [\sigma_0(1+\alpha_{el})]^2R_{H_0}}{[\sigma_i(1+2\alpha_{el})+2\sigma_0]^2} \tag{4}$$

where R_{H_0} and R_{H_i} are the Hall coefficients for the host and the inclusion, respectively.

These CMAs give different predictions for $A_{1-x}B_x$ and $B_{1-x}A_x$ at a given volume fraction. This might imply that certain physical variables may still be missing in the formulation. To address this difference and to obtain a good fit with experimental data within the volume fraction ranging from 0 to 1, an empirical EMA-type formulation is introduced. It is assumed that the effective properties obtained from CMA for host A doped with particle B ($A_{1-x}B_x$) and for host B doped with particle A ($B_{1-x}A_x$) are two different materials. These two properties can then be used in the following empirical EMA-type equation to fit experimental data:

$$\phi_1\frac{X_1^2 - X_e^2}{X_1^2 - f_BX_e^2} + \phi_2\frac{X_2^2 - X_e^2}{X_2^2 - f_AX_e^2} = 0 \tag{5}$$

where X_1 and X_2 are the effective properties for $A_{1-x}B_x$ and $B_{1-x}A_x$, respectively, ϕ_1 and ϕ_2 are their respective volume fractions, and f_A and f_B are the dimensionality parameters defined in standard EMA formulations, but here used as fitting parameters, assuming that the dimensionality differs for X_1 and X_2. This is a quadratic equation of $Y_j = X_j^2$ where j = 1, 2, and e. It has two analytical solutions given by:

$$Y_j = \frac{1}{2A}\left(-B \pm \sqrt{B^2 - 4AC}\right) \tag{6a}$$

$$A = f_A + \gamma f_B, \gamma = \frac{\phi_2}{\phi_1} \tag{6b}$$

$$B = (1-\gamma f_B)Y_1 + (\gamma - f_A)Y_2 \tag{6c}$$

$$C = -(1+\gamma)Y_1Y_2 \tag{6d}$$

in which X_e is f_{a_Sd}, a_{SA}, a_{SB}, and m_{a_S} are the empirical parameters to be determined through correlation with experimental data.

In the current CMA of the Hall coefficient, only the electrical barrier resistance is accounted for. It is given by:

3 Results

Results for undoped Ge–Si alloys which have also been extensively investigated through experiments are presented in Fig. 2. The parameters used for the calculation[3] are given in Table 1. Figure 2 compares the results of the CMA, Eq. (1a), for $Ge_{1-x}Si_x$ and $Si_{1-x}Ge_x$ and the empirical EMA-type formulation, Eq. (5), with the experimental data[17]. The particle size used for these results is 66 nm. The parameters used for the distribution function of the host–particle interface density are r_A = 0.5, r_B = 0.175, and m_h = 0.7. The parameter used for the distribution function of the thermal barrier resistance is m_k = 0.975. The coefficient of the electrical barrier resistance is $\alpha_{el}^0 = 0.8$, and its distribution function is $f_{sd} = 1$. The Seebeck coefficient ratio is a_S = 0. Figure 2b shows the distribution functions used for the thermal barrier resistance and the host–particle interface density. Figure 2a clearly shows that the introduction of the distribution functions improves the CMA's prediction considerably. These predictions are converged to the thermal resistivity of the host medium and the particle at atomic fractions of 0 and 1, respectively. The results of the CMA for $Ge_{1-x}Si_x$ and $Si_{1-x}Ge_x$, and the empirical EMA, are nearly the same and all agree well with the experimental data up to the atomic fraction of 0.25. However, there exist considerably differences between the CMA predictions for $Ge_{1-x}Si_x$ and $Si_{1-x}Ge_x$ within a large portion of atomic fractions. The empirical EMA-type formulation resolves these differences and gives a unique prediction at a given atomic fraction ranging from 0 to 1. As showed in Fig. 2a, the thermal resistivity predicted by the empirical EMA agrees very well with the experimental data within the atomic fraction range from 0 and 1 using f_A = 25.5 and f_B = 0.25. It can also be observed that within this range of atomic fraction, the CMA for $Ge_{1-x}Si_x$ and the empirical

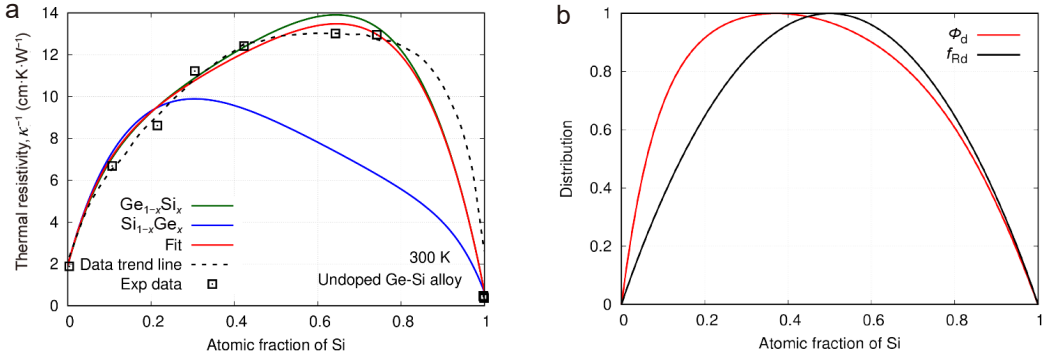

Figure 2 (a) Comparisons of the effective thermal resistivity predicted by CMA for $Ge_{1-x}Si_x$ and $Si_{1-x}Ge_x$ and the empirical EMA with the experimental data. (b) Distribution functions for the host–particle interface density, Φ_d, and the thermal barrier resistance, f_{Rd}.

Table 1 Thermal properties for undoped silicon and germanium

Material	Bulk thermal conductivity (W·m^{-1}·K^{-1})	Heat capacity (10^6 J·m^{-3}·K^{-1})	Phonon group velocity (m·s^{-1})	Bulk mean free path (nm)
Si	150	0.93	1804	268
Ge	51.7	0.87	1042	171

EMA are nearly the same, except within the peak portion.

Figure 3 presents the transport properties predicted by the CMAs for $Ge_{1-x}Si_x$ and $Si_{1-x}Ge_x$ and the empirical EMA for an *n*-type Ge–Si alloy having a carrier concentration of 1.5 × 10^{20} electrons/cm^3. The parameters[17–24] used for the calculation are given in Table 2. The phonon group velocity was calculated using the Debye expression[25], $v = (k_B/\hbar)(6\pi^2)^{-1/3}a\theta_D$, where a is the cube root of the atomic volume, and the Debye temperature $\theta_D = 4.19 \times 10^{-8}\ G/(a^{3/2}M^{1/2})$ in which M is the mean "gram

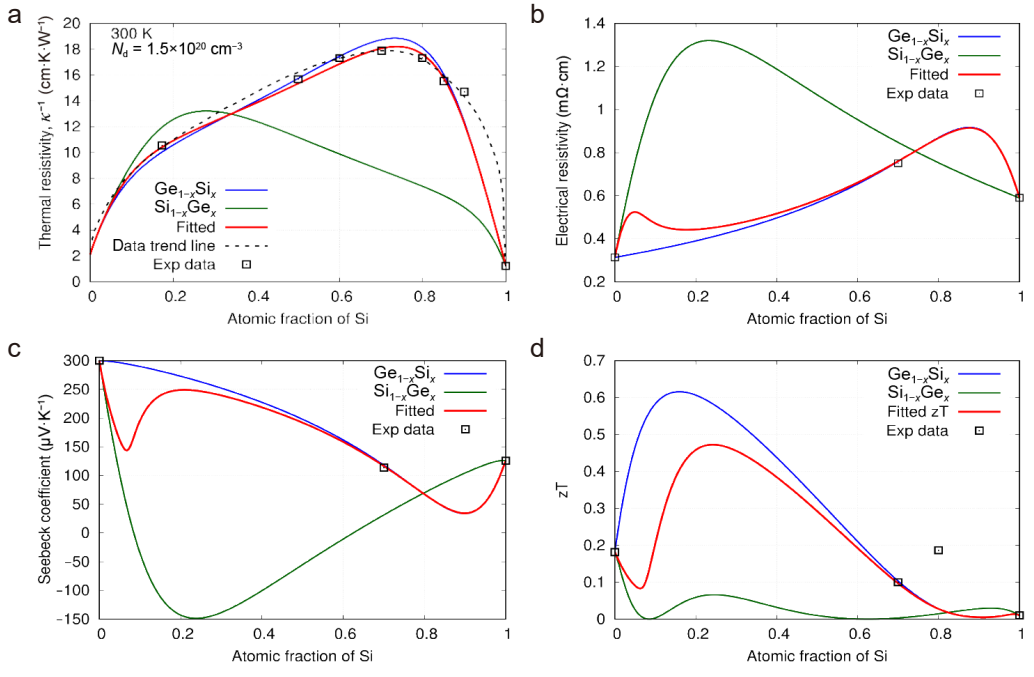

Figure 3 Comparisons of the effective transport properties predicted by CMA for $Ge_{1-x}Si_x$ and $Si_{1-x}Ge_x$ and the empirical EMA with experimental data. (a) Thermal resistivity. (b) Electrical resistivity. (c) Seebeck coefficient. (d) Figure of merit.

Table 2 Properties of the doped *n*-type silicon and germanium

Materials	Bulk thermal conductivity (W·m^{-1}·K^{-1})	Heat capacity (10^6 J·m^{-3}·K^{-1})	Phonon group velocity (m·s^{-1})	Bulk MFP (μm)	Seebeck coefficient (μV·K^{-1})	Electrical conductivity (10^5 S·m^{-1})
Si	82.42	1.56	5858	158.5	125.5	1.696
Ge	47.5	1.713	3519	83.2	300	2.188

atomic weight" of alloy, G is a function of the elastic constants. G = 1.017 for Germanium and 1.033 for silicon[17, 26]. The phonon MFP was back calculated from the specific heat, the phonon group velocity, and the thermal conductivity using the kinetic equation, Eq. (1c). For a more rigorous calculation, it could be extracted from the expressions of the Seebeck coefficient, the electrical conductivity, and the thermal conductivity obtained from the Boltzmann transport equation for electron and phonon in combination with those measured properties. These will give three equations containing the Fermi energy level, the electron relaxation time, and the phonon scattering rate as the unknowns. These equations need to be solved iteratively. Figure 4 shows the distribution functions, Φ_d, f_{Rd}, f_{asd}, and f_{sd}, used for the calculations.

Figure 3a compares the thermal conductivity obtained from the CMA, Eq. (1), and the empirical EMA, Eq. (5), with the experimental data[17]. The CMA results for $Ge_{1-x}Si_x$ and $Si_{1-x}Ge_x$ agree well only within the atomic fraction range from 0 to 0.15. They then differ considerably for most of the remaining atomic fractions. The empirical EMA resolves their differences and gives a unique prediction for a given atomic fraction ranging from 0 and 1. It can be noticed that the CMA for $Ge_{1-x}Si_x$ and the empirical EMA are nearly the same except within the peak portion and they all agree very well with the experimental data. Figure 3b shows the comparisons of the electrical resistivity. The CMAs for $Ge_{1-x}Si_x$ and $Si_{1-x}Ge_x$ differ considerably within the entire range of atomic fraction except those near their interception point. Results of the empirical EMA agree well with both the prediction of the CMA for $Ge_{1-x}Si_x$ and the experimental data (only one data point can be extracted). Figure 3c compares the Seebeck coefficients computed by the CMA for $Ge_{1-x}Si_x$ and $Si_{1-x}Ge_x$ and the empirical EMA with the experimental data. The trends observed in the Seebeck coefficients are very similar to those of the electrical resistivity. The CMAs for $Ge_{1-x}Si_x$ and $Si_{1-x}Ge_x$ are considerably different within the entire range of atomic fractions, except at their interception point. Results of the empirical EMA agree with the CMA predictions for $Ge_{1-x}Si_x$ and experimental data within the atomic range between 0.2 and 1. They differ between 0 and 0.2 within which CMA predictions for $Ge_{1-x}Si_x$ and $Si_{1-x}Ge_x$ differ significantly. Figure 3d shows the comparisons of the figure of merits. Since CMA for $Ge_{1-x}Si_x$, and the empirical EMA agree well with the experimental data for the thermal resistivity, the electrical resistivity, and the Seebeck coefficient, a very good agreement among them in the figure of merit can be expected. However, owing to the significant differences in the CMA predictions for $Ge_{1-x}Si_x$ and $Si_{1-x}Ge_x$, the empirical EMA only agree well with the CMA for $Ge_{1-x}Si_x$ within the atomic fraction range between 0.5 and 1.

Figure 5 shows the electron Hall mobility computed by the CMAs for $Ge_{1-x}Si_x$ and $Si_{1-x}Ge_x$, and the empirical EMA compared with the experimental data. The data point at the atomic fraction of 0.7 is from Ref [17] and that at 0.8 is the modeled result from Ref [26]. Since the interface effects are not accounted for in the Hall coefficient formulation, these predictions agree not quite well with the experimental data as those for the thermal and the electrical resistivity and the Seebeck coefficient. Because the large differences in the CMA predictions for $Ge_{1-x}Si_x$ and $Si_{1-x}Ge_x$, the empirical EMA agree well with the CMA for $Ge_{1-x}Si_x$ only within the atomic fraction range between 0.3 and 1.

4 Discussion

Application of the smeared property approximation at the interface between the continuous medium and its inclusion can address the discontinuity problem in field variables, which currently was not considered in continuum medium formulations. This approach can extend the application of the continuum medium approximation of transport properties for inhomoge-

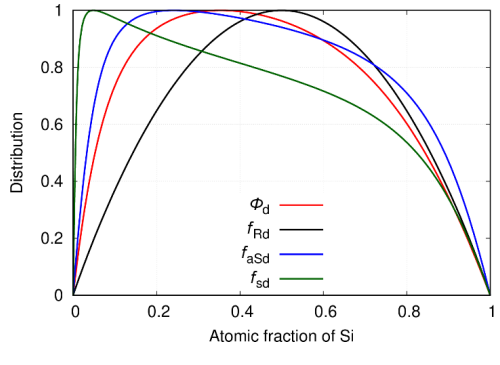

Figure 4 Distribution functions for the host–particle interface density, Φ_d, thermal barrier resistance, f_{Rd}, electrical barrier resistance, f_{sd}, and the Seebeck coefficient ratio, f_{asd}.

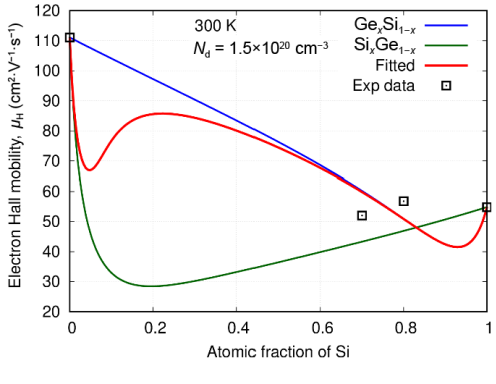

Figure 5 Comparisons of the effective electron Hall mobility predicted by CMA for $Ge_{1-x}Si_x$ and $Si_{1-x}Ge_x$ and empirical EMA with the experimental data.

neous materials to nanostructured composites. The smeared property approximation introduces the interface parameters, i.e., the thermal and the electrical barrier resistance and the Seebeck coefficient ratio, into CMA formulations. Consequently, the approximated properties are not bounded by those of the host medium and the particle of a composite as standard EMAs. The introduction of distribution functions for the host–particle interface density, the thermal and the electrical barrier resistance, and the Seebeck coefficient ratio results in CMA predictions converging to the properties of the host medium and the particle at the atomic fractions of 0 and 1, respectively, and improves the predictions considerably within the entire range of atomic fractions. However, there still exist differences in the CMA predictions for $Ge_{1-x}Si_x$ and $Si_{1-x}Ge_x$ at a given atomic fraction. The proposed empirical EMA resolves those differences and gives a unique prediction at a given atomic fraction ranging from 0 to 1. As Fig. 2 showed for undoped Ge–Si alloys, the CMA for $Ge_{1-x}Si_x$ gives the predictions of the thermal resistivity of Ge at the atomic fraction of 0 and that of Si at 1 and the predictions agree very well with the experimental data within those fraction range. The CMA for $Si_{1-x}Ge_x$ also predicts the thermal resistivity of Ge at the atomic fraction of 0 and that of Si at 1. The predictions between 0 and 0.2 agree very well with those of CMA for $Ge_{1-x}Si_x$. For larger atomic fractions, however, the predictions differ considerably. The empirical EMA resolves these differences and gives a unique prediction for a given atomic fraction ranging from 0 to 1, which agree very well with experimental data. It can be noticed that the predictions of the empirical EMA and the CMA for $Ge_{1-x}Si_x$ are nearly the same, except at the peak portion. This indicates that CMA for $Ge_{1-x}Si_x$ along can be used for the predictions of nanostructured composites.

Figure 3 shows the results for the thermal resistivity, the electrical resistivity, and the Seebeck coefficient of *n*-type doped Ge–Si alloys with a carrier concentration of 1.5×10^{20} electrons/cm^3. The results for thermal resistivity showed in Fig. 3a are quite similar to those for undoped Ge–Si alloys (Fig. 2). But the particle size used for these calculations is 8.75 nm and the distribution functions used are different as showed in Fig. 4. From Figs. 2a and 3a, it can be noticed that the thermal resistivity increases as the particle size becomes smaller and the interface density becomes larger. This can be reasoned that as the doping concentration increases the host–particle interface density also increases. To increase the interface density, the particle size must be small since it is an inverse proportion to the interface density[3].

Figure 3 also shows the predicted results for the electrical resistivity, the Seebeck coefficient, and the figure of merit. These results indicate that the predicted properties by the CMA for $Ge_{1-x}Si_x$ are consistently agree with the empirical EMA and experimental data. The differences between these two predictions within a certain range of atomic fractions are mainly resulted from the prediction differences between CMA for $Ge_{1-x}Si_x$ and $Si_{1-x}Ge_x$. This suggests that CMA for $Ge_{1-x}Si_x$ alone can predict the properties of nanostructured composites. It needs to point out that CMAs for $Ge_{1-x}Si_x$ and $Si_{1-x}Ge_x$ differ only in their use of host and particle and their property ratios (i.e., κ_i/κ_0, σ_i/σ_0, and α_i/α_0). These rules should be followed for CMA.

Missing of a distribution function for electron Hall mobility in the current CMA formulation results in the predictions that are not correlated with experimental data. The predicted Hall mobilities do not agree well with the experimental data (Fig. 5). More understanding of the interface effect on Hall mobility, which is beyond the scope of this study, may be needed before introducing the distribution function into CMA. Furthermore, unlike the thermal conductivity, the electrical conductivity, the Seebeck coefficient, and the Hall mobility in the current CMA are independent of the host–particle interface density and particle size. By analogizing to the thermal conductivity, the Drude model may be used to calculate the electrical conductivity by modifying the electron mobility to include the effects of particle size and interface density.

Using the distribution functions showed in Fig. 4, the effects of the interface parameters on the transport properties were studied with respect the Seebeck coefficient ratio, a_S, and the coefficient of electrical barrier resistance, α_{el}^0. These results are shown in Fig. 6.

Figure 6a compares the variations in the effective Seebeck coefficients with the atomic fraction of Si for different a_S under a given α_{el}^0. As a_S increases from −2.75 to 2.75, the effective Seebeck coefficient decreased. At $a_S = 2.75$, the α_p corresponded to the experimental data at the atomic fraction of 0.7, which is lower than those of Ge and Si. Since $a_S = \alpha_0/\alpha_B$, the interface Seebeck coefficient, α_B, needs to be smaller than that of the host medium to lower the effective Seebeck coefficient. This applies to all the a_S that > 0.297. At $a_S = 0$, no interface effect observed with respect to Seebeck coefficient. It can be understood either a perfect interface or a significantly large interface Seebeck coefficient. The later interpretation implies that the effective Seebeck coefficient can only vary between those of Ge and Si when the interface Seebeck coefficient is considerably large. If $a_S < 0$ i.e., the interface α_B has opposite sign to that of α_0 does, α_p would be larger than that of Si or Ge, depending on the magnitude of a_S and the atomic fraction of Si. This is an interesting result since it shows a possible way to increase the Seebeck coefficient of a nanos-

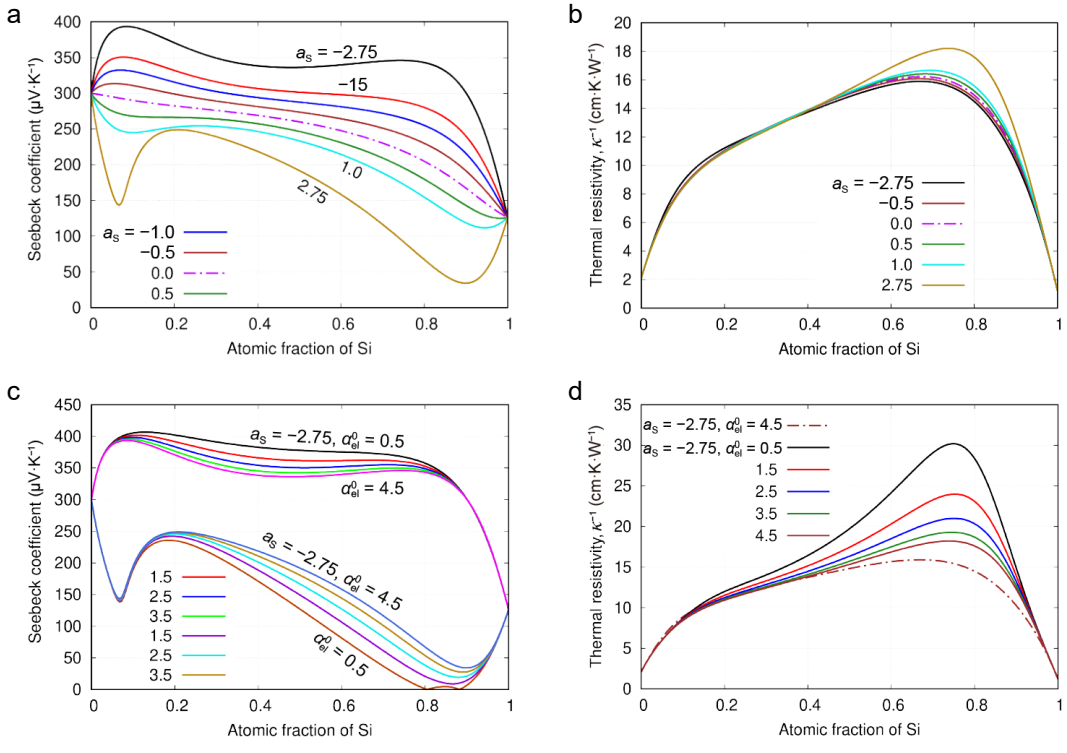

Figure 6 Effects of interface parameters, a_S and α^0_{el}, on the transport properties. Effect of a_S on (a) Seebeck coefficient and (b) thermal resistivity. Effect of α^0_{el} on (c) Seebeck coefficient and (d) thermal resistivity.

tructured composites through interface parameters.

Figure 6b shows the changes in the effective thermal resistivity as a_S increases from 2.75 to 2.75. For $a_S < 0$, the effect of α_{a_S} on the thermal resistivity is minimal, as showed for $a_S = -2.75$ and -0.5. The corresponding thermal resistivity of the remaining negative values of a_S overlapped with each other and are difficult to distinguish. For $a_S > 0$, the effective thermal resistivity increases with a_S. These changes in α_p and κ_p with a_S are inconsistent with those for bulk materials for which as the Seebeck coefficient increases, the thermal conductivity in general decreases.

Figure 6c shows the effect of the coefficient of electrical barrier resistance on α_p for a fixed a_S. For a_S = 2.75, α_p increases as α^0_{el} increases from 0.5 to 4.5. Since the electrical resistivity also increases with α^0_{el}, the increase of α_p with α^0_{el} consistents with the intrinsic relationship between α and σ of bulk materials. For $a_S = -2.75$, α_p decreases as α^0_{el} increases from 0.5 to 4.5. These results are typical for the large negative a_S. Considering that the electrical resistivity is basically independent of a_S for CMA and that the electrical resistivity increase with α^0_{el}, these results are inconsistent with the common intrinsic relationship between α and σ of bulk materials.

Figure 6d shows the effect of the electrical barrier resistance on the thermal resistivity for a fixed a_S. As previously discussed, for $a_S < 0$, the effect of α^0_{el} on the thermal resistivity is minimal, only the results for $a_S = -2.75$ and $\alpha^0_{el} = 4.5$ is showed. For a_S = 2.75, the effective thermal resistivity decreases as α^0_{el} increases from 0.5 to 4.5. Since the electrical resistivity increases with α^0_{el}, the decrease in the thermal resistivity with α^0_{el} is inconsistent with the common intrinsic relationship between σ and κ of bulk materials. However, this is also an interesting result because it shows a possible way to optimize the thermal and the electrical resistivity by manipulating the barrier resistance.

5 Conclusion

A continuum medium approximation of the transport properties of an inhomogeneous composite can be developed using a smeared property approximation at the interface between a continuous medium and its inclusion, along with the perturbation approximation. The CMA can introduce the interface parameters, including the thermal and the electrical barrier resistance and the Seebeck coefficient ratio, in the formulation to account for their effects on the transport properties of nanostructured composites. However, these interface parameters also lead to the predictions to deviate from the inclusion properties at the volume fraction of 1, thereby increasing the differences in the CMA predictions for $A_{1-x}B_x$ and $B_{1-x}A_x$. The introduction of the new distribution functions for the interface parameters into CMA formulations can address the non-converging predictions and considerably improve the predictions. The empirical EMA combines the CMA

predictions from both $A_{1-x}B_x$ and $B_{1-x}A_x$ to resolve the differences in these predictions and give a unique prediction that can agree very well with experimental data for a given atomic fraction of the inclusion ranging from 0 to 1.

The study of the effects of interface parameters on the transport properties revealed that the Seebeck coefficient ratio needs to be small to minimize the reduction in the effective Seebeck coefficient of the composite. If the sign of the interface Seebeck coefficient becomes opposite to that of the host Seebeck coefficient, the effective Seebeck coefficient can exceed that of the host medium. The study further showed that increase in the electrical barrier resistance can increase the electrical resistivity and lower the thermal resistivity, inconsistent with the common intrinsic relationship of bulk materials. These results suggested potential ways to improve the transport properties. Therefore, it can be concluded that the efficiency of nanostructured composite can potentially be further improved by optimizing the interface parameters.

Acknowledgements

None.

Author contribution statement

Zhang TG confirms being the sole contributor of this work and has approved it for publication.

Data availability

The data that supports the findings of this study is available from the corresponding author upon reasonable request.

Declaration of competing interest

The author delares no conflict of interests in this work.

Funding

None.

Use of AI statement

None.

References

[1] Kapitza, P. L. (1941). Heat Transfer and Superfluidity of Helium II. *Physical Review* 60, 354–355.

[2] Nan, C. W., Birringer, R., Clarke, D. R., Gleiter, H. (1997). Effective thermal conductivity of particulate composites with interfacial thermal resistance. *J. Appl. Phys.* 81, 6692–6699.

[3] Minnich, A., Chen, G. (2007). Modified effective medium formulation for the thermal conductivity of nanocomposites. *Appl. Phys. Lett.* 91, 073105.

[4] Poon, S. J., Limtragool, K. (2011). Nanostructure model of thermal conductivity for high thermoelectric performance. *J. Appl. Phys.* 110, 114306.

[5] Hao, F., Fang, D. N., Xu, Z. P. (2012). Thermal transport in crystalline Si/Ge nano-composites: Atomistic simulations and microscopic models. *Appl. Phys. Lett.* 100, 091903.

[6] Sonntag, J. (2009). Thermoelectric power in alloys with phase separation (composites). *J. Phys.: Condens. Matter* 21, 175703.

[7] Kyratsi, T., Hatzikraniotis, E., Ioannou, M., Chung, D. Y., Tsiaoussis, I. (2011). Seebeck and thermal conductivity analysis in amorphous/crystalline β-$K_2Bi_8Se_{13}$ nanocomposite materials. *J. Appl. Phys.* 110, 033713.

[8] McLachlan, D. S. (1985). Equation for the conductivity of metal-insulator mixtures. *J. Phys. C: Solid State Phys.* 18, 1891–1897.

[9] Bergman, D. J., Levy, O. (1991). Thermoelectric properties of a composite medium. *J. Appl. Phys.* 70, 6821–6833.

[10] Sharma, P. A., Sugar, J. D., Medlin, D. L. (2010). Influence of nanostructuring and heterogeneous nucleation on the thermoelectric figure of merit in $AgSbTe_2$. *J. Appl. Phys.* 107, 113716.

[11] Gesele, G., Linsmeier, J., Drach, V., Fricke, J., Arens-Fischer, R. (1997). Temperature-dependent thermal conductivity of porous silicon. *J. Phys. D: Appl. Phys.* 30, 2911–2916.

[12] Yu, J. K., Mitrovic, S., Tham, D., Varghese, J., Heath, J. R. (2010). Reduction of thermal conductivity in phononic nanomesh structures. *Nat. Nanotechnol.* 5, 718–721.

[13] Lee, H., Vashaee, D., Wang, D. Z., Dresselhaus, M. S., Ren, Z. F., Chen, G. (2010). Effects of nanoscale porosity on thermoelectric properties of SiGe. *J. Appl. Phys.* 107, 094308.

[14] Tao, H. L., Chen, G., Lian, C., Liu, H. L., Coppens, M. O. (2022). Multiscale modeling of ion transport in porous electrodes. *AIChE J.* 68, e17571.

[15] Ryden, D. J. (1974). The effects of isolated inclusions upon the transport properties of semiconductors. *J. Phys. C: Solid State Phys.* 7, 2655–2669.

[16] Bartkowiak, M., Mahan, G. D. (2001). Heat and electricity transport through interfaces. *Semicond. Semimetals* 70, 245–271.

[17] Dismukes, J. P., Ekstrom, L., Steigmeier, E. F., Kudman, I., Beers, D. S. (1964). Thermal and electrical properties of heavily doped Ge-Si alloys up to 1300°K. *J. Appl. Phys.* 35, 2899–2907.

[18] Okhotin, A. S., Pushkarskii, A. S., Gorbachev, V. V. (1972). Thermophysical Properties of Semiconductors. Moscow: "Atom" Publ. House.

[19] Piesbergen, U. Z. (1963). Die durchschnittlichen atomwärmen der A^{III} B^{V}-Halbleiter AlSb, GaAs, GaSb, InP, InAs, lnSb und die atomwärme des elements germanium zwischen 12 und 273°K3. *Z. für Naturforsch. A* 18a, 141–147.

[20] Cuttriss, D. B. (1961). Relation between surface concentration and average conductivity in diffused layers in germanium. *Bell Syst. Tech. J.* 40, 509–521.

[21] Fistul, V. I., M. I. Iglitsyn, and E. M. Omelyanovskii. (1962). Mobility of electrons in germanium strongly doped with arsenic. *Soviet Physics-Solid State* 4, 784–785.

[22] Thurber, W. R., Mattis, R. L., Liu, Y. M., Filliben, J. J. (1981). Semiconductor measurement technology: The relationship between resistivity and dopant density for Phosphorus and Boron doped Silicon. Washington: National Bureau of Standards 400–64.

[23] Geballe, T. H., Hull, G. W. (1955). Seebeck effect in silicon. *Phys. Rev.* 98, 940–947.

[24] Xu, Q., Zhou, J. W., Liu, T. H., Chen, G. (2021). First-principles study of all thermoelectric properties of Si-Ge alloys showing large phonon drag from 150 to 1100 K. *Phys. Rev. Appl.* 16, 064052.

[25] Steigmeier, E. F., Abeles, B. (1964). Scattering of phonons by electrons in germanium-Silicon alloys. *Phys. Rev.* 136, A1149–A1155.

[26] Vining, C. B. (1991). A model for the high-temperature transport properties of heavily doped *n*-type Silicon-germanium alloys. *J. Appl. Phys.* 69, 331–341.